Environmental Science
Processes & Impacts

Accepted Manuscript

ROYAL SOCIETY OF CHEMISTRY

rsc.li/process-impacts

Environmental Impact

Despite extensive research on the aggregation behavior of nanoparticles in aquatic systems, there is only limited information available about manganese oxides (MnO_2) that play a critical role in controlling the mobility and concentration of heavy metals in the environment. It is first paper to explore the aggregation behavior of a poorly-crystalline MnO_2 (δ-MnO_2) under various water conditions. The aggregation state of δ-MnO_2 is strongly dependent on the solution property, and it subsequently affects the sorption performance toward Cu(II). In the light, the adsorbed Cu(II) can be released from δ-MnO_2 surface via photoinduced dissolution of MnO_2. This work will provide valuable insights into heavy metal-mineral interactions in response to common environmental stimuli.

Environmental Science: Processes & Impacts RSCPublishing

PAPER

Sorption behavior of heavy metals on poorly-crystalline manganese oxides: Role of water conditions and light†

Cite this: DOI: 10.1039/xoxxoooooox

Received ooth January 2014,
Accepted ooth January 2014

DOI: 10.1039/xoxxoooooox

www.rsc.org/

Eun-Ju Kim [a], Jungwon Kim [b], Sung-Chan Choi [b], and Yoon-Seok Chang [a,]*

The objective of this study was to determine the effects of solution properties and UV light on the metal uptake and release in a nanosized, poorly crystalline manganese oxide (δ-MnO_2) system. The results from synthetic water matrices revealed that the aggregation state was strongly affected by ionic strength, Ca^{2+}, and humic acid, and the particle aggregation subsequently changed the ability of δ-MnO_2 to adsorb and sequester heavy metal ions (Cu(II)). The extent of Cu(II) uptake onto δ-MnO_2 exhibited a negative correlation with the attachment efficiency value, which suggested that a lower sorption capacity could be achieved under aggregation-inducing conditions. Upon exposure to light, the adsorbed Cu(II) was released from the δ-MnO_2 surface via photoinduced dissolution of MnO_2. The concentration of Cu(II) desorbed was substantially higher when humic acid was present together with Ca^{2+}. The present investigation enables us to better understand the adsorption-desorption processes of heavy metals occurring at MnO_2−solution interface in response to common environmental stimuli.

Introduction

Manganese oxides (MnO_2), which are ubiquitous in the subsurface environment, have attracted much attention owing to their versatile use in industrial applications and environmentally important role in element cycling.[1] Studies with real and model systems have suggested that the remarkable ion exchange capacities and high sorption abilities of MnO_2 minerals control the mobility and concentration of heavy metals and other inorganic species in sediments, soils, and associated aqueous media.[2-5] In nature, MnO_2 occurs in several different polymorphs with distinct crystalline structures, chemical compositions, and properties. A large portion of MnO_2 found in many geochemical environments is poorly crystalline forms, which are more reactive than the well-crystallized counterparts.[6] For these reasons, we plan to investigate the reactivity of MnO_2 phases with poor crystallinity.

It is generally accepted that both engineered and naturally occurring nanoparticles interact with the surrounding aqueous conditions and typically undergo aggregation.[7,8] Solution properties (i.e., ionic strength, complexing agents, and natural organic matter (NOM)) alter the interfacial morphology, charge, and hydrophobicity, which determine whether the particles aggregate or disperse.[9-11] Nanoparticle aggregation has significant consequences regarding the mobility, toxicity, and reactivity. In previous studies, aggregation has been shown to decrease the nanoparticle reactivity toward organohalide contaminants and heavy metals.[12,13] They proposed that the aggregation led to loss of available surface area and formation of compact nonporous structure, which reduced the reaction properties of nanoparticles. In this respect, the studies on how the environmental conditions influence the aggregation state of nanomaterials should be essential part of the general characterization for assessing reactivity. However, very little information is available on the aggregation behavior of nanosized MnO_2 and the impact on its sorption performance for toxic metals.

In addition to water conditions, light can also contribute to the changes in the size and morphology of MnO_2 because it is recognized to be photosensitive due to its semiconducting nature.[14] Under light exposure, the metallic/oxide nanoparticles undergo several transformation processes, such as dissolution, growth, and reversible aggregation.[15-17] The light-induced dissolution of MnO_2 plays critical roles in the cycling and bioavailability of manganese.[18] However, it may cause other environmental concerns resulting from the release of adsorbed organic and inorganic (i.e. heavy metal) contaminants back into the environment via the dissolution process of MnO_2. Although the effect of light on the dispersion of bare nanoparticles has occasionally been investigated, photoinduced reactions on heavy metal-bearing ones are poorly understood to date.

Herein we thoroughly explored the adsorption and desorption of Cu(II) (as a model of heavy metals) on nanosized MnO_2 under a variety of solution conditions in the absence and presence of light. A poorly crystalline, layered structure MnO_2 (δ-MnO_2) was chosen considering its high abundance in natural settings.[19] The synthetic water matrices were achieved by varying pH (H^+), alkaline and alkaline earth metal (Na^+ and

Ca^{2+}) concentrations, and the presence of humic acid. The results from this study provide insight into the metal-mineral interactions in response to environmental stimuli based on the mechanisms of aggregation and photoinduced dissolution.

Materials and methods

Chemicals and materials

All chemicals used in the experiments were of analytical grade and purchased from Sigma-Aldrich. Electrolyte (NaCl and $CaCl_2$) stock solutions were prepared with deionized (DI) water. Humic acid (HA) stock solutions were prepared by dissolving Suwannee River humic acid (SRHA, International Humic Substances Society) in DI water, followed by filtration through a 0.45-μm cellulose acetate membrane (ADVANTEC) under vacuum.

δ-MnO_2 was synthesized according to a previously published method.[6] Briefly, a manganese(II) nitrate solution was added dropwise to an alkaline permanganate solution under stirring, which resulted in a final Mn(II): Mn(VII): OH mole ratio of 3:2:4. The resulting suspension was washed three times with DI water using centrifugation. To prevent possible dehydration of the surface, the as-prepared δ-MnO_2 was stored in DI water at all times.

Characterization

The size and morphology of δ-MnO_2 were analyzed with transmission electron microscopy (TEM, JEOL JEM-2200FS). The X-ray diffraction (XRD) pattern was recorded using a PANalytical X'Pert diffractometer with Cu Kα radiation (λ = 0.154 nm). The UV-Vis diffuse reflectance absorption spectrum (UV-DRS) of δ-MnO_2 was obtained using a UV-2600 spectrophotometer (Shimadzu) equipped with a diffuse reflectance accessory, and $BaSO_4$ was used as the reference. The electrophoretic mobility (EPM) and hydrodynamic size in the diluted suspension were measured by an ELS-8000 (Otsuka). The EPMs were further converted to ζ-potential based on the Smoluchowski equation. The surface topography was obtained from height images collected using an atomic force microscope (AFM, Bruker Nanoscope V) in the tapping mode. For the AFM analysis, a drop of the particle suspension was spread onto a mica substrate surface via spin coating and dried overnight at room temperature.

Determination of aggregation kinetics

The aggregation experiments were conducted on a diluted δ-MnO_2 suspension (10 mg/L) containing electrolytes and/or HA for a period of time to obtain an approximately 30% increase in the hydrodynamic diameter of δ-MnO_2.

The aggregation kinetics under specific conditions are characterized by an attachment efficiency, α. The attachment efficiency is determined by normalizing the initial aggregation rate in a given solution condition to the initial rate under favorable (fast) aggregation conditions:[20]

$$\alpha = \frac{k}{k_{fast}} = \frac{\left(\frac{\mathrm{d}D_h(t)}{\mathrm{d}t}\right)_{t\to 0}}{\left(\frac{\mathrm{d}D_h(t)}{\mathrm{d}t}\right)_{t\to 0,fast}} \qquad (1)$$

Cu(II) sorption test

Adsorption experiments were conducted at an unadjusted pH (6.2 ± 0.2) and room temperature. All of the experiments were performed in duplicate. Typically, 10 mg of the as-prepared δ-MnO_2 was added to 20 mL of 10 mg/L Cu(II) solution. After 30 min, the residual Cu(II) concentration in the solution was determined using inductively coupled plasma-atomic emission spectroscopy (ICP-AES, IRIS-AP).

In order to examine the effects of pH, monovalent and divalent electrolytes, and HA on the sorption of Cu(II), the solutions were varied with 0.1 M HCl or 0.1 M NaOH, NaCl, $CaCl_2$, and HA, respectively.

Dissolution experiment

After the Cu(II) sorption test in DI water without electrolytes and HA, Cu(II)-bearing δ-MnO_2 was separated from the solution by centrifugation, and then redispersed in the solution containing NaCl, $CaCl_2$, HA, NaCl/HA, or $CaCl_2$/HA. After 10 h under dark or irradiated conditions, the concentrations of dissolved Cu and Mn in the solution were measured by ICP-AES. To investigate the effect of light irradiation on the desorption of Cu(II), a 300-W Xe arc lamp (Oriel) was used as a light source. The light beam was passed through a 5-cm IR water filter and a cutoff filter (λ > 320 nm) and focused onto a cylindrical Pyrex reactor (30 mL) with a quartz window. The

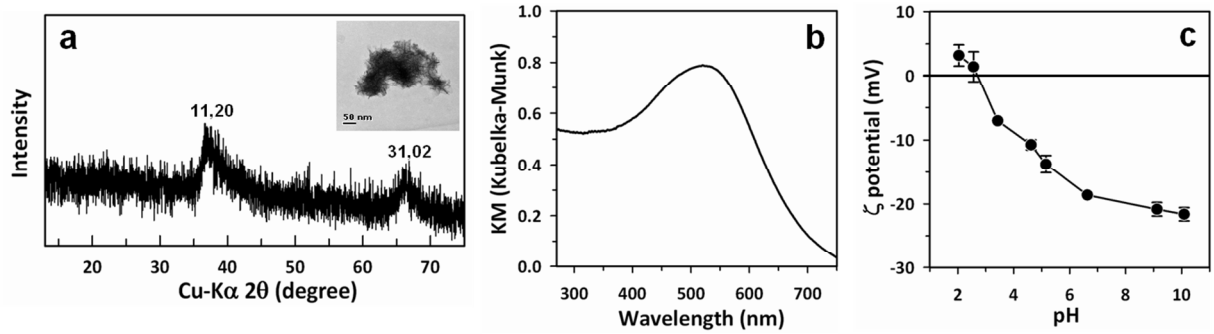

Fig. 1 Characterization of δ-MnO_2. (a) XRD pattern (inset: TEM image); (b) UV-Vis DRS spectrum; (c) ζ potentials as a function of pH in 1 mM NaCl. The 11,20 and 31,02 diffraction bands indicate the reflection pairs 200, 110 and 310, 020.

incident light intensity was about 75 mW/cm^2, which was slightly lower than an average value of natural sunlight (100 mW/cm^2).[21]

Results and discussion

Characterization of δ-MnO_2

The TEM image of the product (inset of Fig. 1a) indicated that small needle-like particles were agglomerated to form spherical structures with a size of 50−100 nm. The crystal phase of synthesized MnO_2 was confirmed by XRD analysis. As shown in Fig. 1a, broad peaks at 2θ = 36.7 and 65.8° in the pattern corresponded to typical δ-MnO_2,[22] and it was considered to be poorly crystalline. The optical DRS spectrum of δ-MnO_2 exhibited a broad band at 400-600 nm (Fig. 1b). This absorption originates from the d−d transition of Mn ions in δ-MnO_2.[23] The ζ potential measurements at different pH values revealed that the isoelectric point (IEP) of δ-MnO_2 was found to be pH 3.2 (Fig. 1c), which was close to the point of zero charge (PZC) obtained from a potentiometric titration.[24] When the pH increased from 2 to 10, the ζ potentials of δ-MnO_2 became more negative. The dependence of surface charge on solution pH indicates the presence of ionizable functional groups (≡ Mn-OH) on the surface. Nevertheless, it is likely that ionization of surface groups is not the only mechanism arising from the surface charge because δ-MnO_2 is negatively charged even under low pH conditions. Another important source of the negative charge of δ-MnO_2 can be the large amount of vacancies within the Mn^{IV} octahedral sheets.[25] It has been determined that the vacant sites account for approximately 6-7% of the total Mn sites.[26,27]

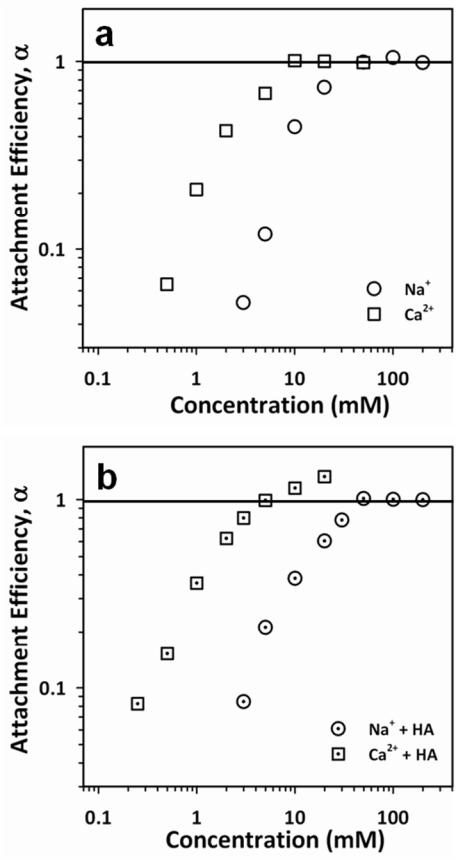

Fig. 2 Attachment efficiencies of δ-MnO_2 as a function of electrolyte concentrations in the absence (a) and presence (b) of HA (1 mg/L DOC) at an unadjusted pH of 6.2 ± 0.2.

Effect of solution conditions on δ-MnO_2 aggregation

The aggregation characteristics of δ-MnO_2 were evaluated in solutions simulating natural aquatic systems at ambient temperature. Fig. S1 shows the electrophoretic mobility (EPM) values of δ-MnO_2 as a function of electrolyte concentration. As compared to the EPM in DI water, the observed values became less negative with increasing electrolyte concentrations because of the charge screening effect by the adsorption of Na^+ or Ca^{2+} on δ-MnO_2. In addition, divalent Ca^{2+} ions were more efficient than Na^+ ions in changing the EPMs of δ-MnO_2, which was consistent with the results reported in the literature.[28-30]

The aggregation kinetics of δ-MnO_2 were studied with NaCl concentrations ranging from 3 to 200 mM and $CaCl_2$ concentrations ranging from 0.5 to 50 mM at pH 6.2 where the particles were negatively charged and quite stable (Fig. 2a). The attachment efficiency, α, calculated from Eq. (1) was employed to quantitatively describe the initial aggregation kinetics of δ-MnO_2. The δ-MnO_2 exhibited two distinct unfavorable (reaction-limited) and favorable (diffusion-limited) aggregation regimes in the presence of both NaCl and $CaCl_2$, which followed the classical Derjaguin-Landau-Verwey-Overbeek (DLVO) theory. In the unfavorable aggregation regime (α < 1), an increase in the electrolyte concentration leads to a corresponding increase in the attachment efficiency. When the electrolyte concentration approaches and exceeds the

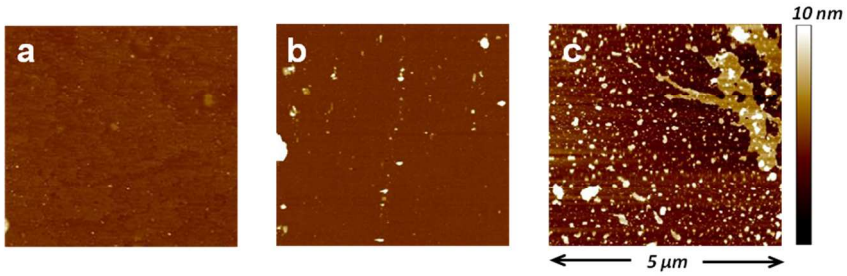

Fig. 3 Representative AFM images of δ-MnO_2 in the absence (a) and presence of (b) Ca^{2+} as well as (c) HA and Ca^{2+}. The concentrations of HA and Ca^{2+} were 1 mg/L DOC and 5 mM, respectively.

critical coagulation concentration (CCC), the electrolyte concentration has no effect on the attachment efficiency. Under these conditions, the electrostatic repulsion force is suppressed and the attractive van der Waals forces dominate between the particles resulting in fast aggregation. The intersection of the two aggregation regimes yields CCC values in the respective electrolytes. The CCC was much smaller for $CaCl_2$ (8.5 mM) than for NaCl (42.1 mM), suggesting that the increase in cation valence had a significant impact on the particle stability. This difference in CCCs is most likely due to the stronger adsorption behavior of Ca^{2+} compared to Na^+ on the δ-MnO_2 surface.[31]

Since humic acid (HA), as a major component of NOM, is found everywhere in natural water, the effect of HA on the aggregation of δ-MnO_2 with Na^+ or Ca^{2+} was also investigated. The HA concentration for all experiments was 1 mg/L as DOC. After addition of HA, the particles showed a slightly less negative EPM than that of bare δ-MnO_2 (Fig. S1). This differed from other studies with TiO_2, Fe_2O_3, and Al_2O_3,[28,32,33] in which HA imparts a negative surface charge to suspended particles. We speculate that the opposite result is ascribed to the different IEP values. At pH 6.2 ± 0.2, the above nanoparticles are neutral or positively charged, whereas δ-MnO_2 is negatively charged. Therefore, the adsorption of HA may reduce the negative charge density of δ-MnO_2 by masking the underlying particle charges, as proposed in Scheme S1.[34] With increasing electrolyte concentrations, the presence of HA made the EPMs less negative, which was interpreted to cause an increased screening of the charge on HA.

In comparison to what was observed in NaCl, the aggregation kinetics of δ-MnO_2 in $CaCl_2$ were greatly affected by the presence of HA. The CCC of 43.5 mM NaCl was similar to that in the absence of HA (42.1 mM), while it decreased from 8.5 mM (without HA) to 4.6 mM $CaCl_2$ (Fig. 2b). At the $CaCl_2$ concentrations above 4.6 mM, the attachment efficiencies were greater than unity. This enhanced aggregation ($\alpha > 1$) of δ-MnO_2 could be ascribed to intermolecular bridging between Ca^{2+} and anionic functional groups of adsorbed/dissolved HA.[35] The resulting HA clusters were subsequently attached to δ-MnO_2 nanoparticles and bridged between them to form larger aggregates. Similar results were also observed in the AFM analysis (Fig. 3). Relatively large aggregates were detected in the mica surface with 5 mM Ca^{2+} and 1 mg/L HA compared to the surface treated with only 5 mM Ca^{2+}. In the literatures,[36,37] enhanced aggregation of nanoparticles in the presence of HA has been reported at higher Ca^{2+} concentrations than that in this study. This discrepancy likely reflects the different concentration ratios between the particles and HA or different particle properties (i.e., pH_{IEP}, size).

Adsorption of Cu(II) in synthetic water matrices

We performed Cu(II) sorption experiments to examine the effects of δ-MnO_2 aggregation on heavy metal uptake by varying water conditions, such as pH, electrolyte concentrations, and presence of HA. Fig. S2 presents the pH dependence of Cu(II) adsorption onto δ-MnO_2 in the range of pH 2.4−9.3. As the pH increased from 2.4 to 6.0, the adsorption efficiency increased from 30 to 99.5%, and it did not change considerably at higher pH values. Increasing the pH results in a higher negative charge density on the surface of δ-MnO_2, thus enhancing the Cu(II) uptake via electrostatic attraction. When the pH exceeds the pH_{IEP} (pH_{IEP} = 3.2, Fig. 1c), the particles are expected to be stable due to interparticle repulsion that prevents aggregation. In contrast, at a pH near the pH_{IEP}, aggregation typically occurs because the particles have a very low charge density. Nevertheless, the adsorption of Cu(II) still occurred at pH < 3.2 implies that there is a certain form of specific adsorption (i.e., inner-sphere complexation),[31] in addition to the electrostatic interaction.

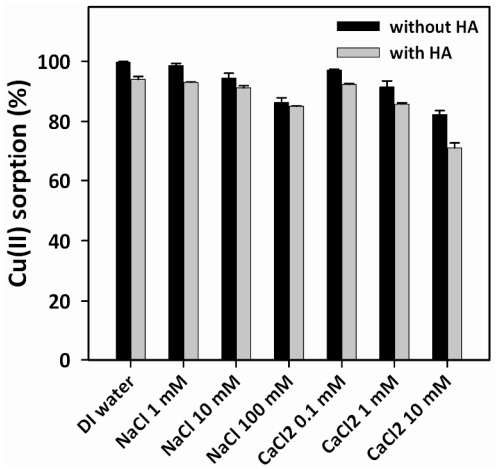

Fig. 4 Effect of electrolyte concentrations in the absence and presence of HA (1 mg/L DOC) on Cu(II) sorption by δ-MnO_2 at pH 6.2 ± 0.2.

Fig. 4 reveals that the sorption percentage of Cu(II) is greatly affected by HA and background electrolytes (NaCl and $CaCl_2$). The presence of HA reduced Cu(II) adsorption on δ-MnO_2, presumably because the remaining HA in solution forms soluble complexes with Cu(II). An increase in the electrolyte

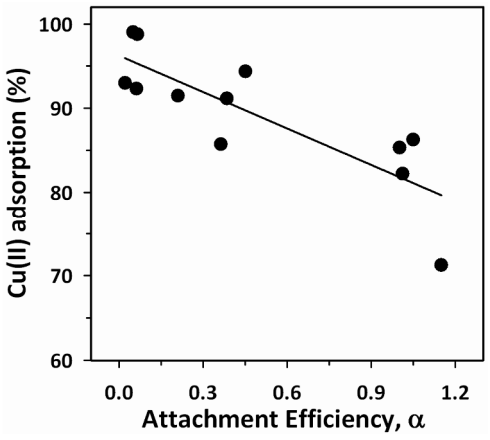

Fig. 5 Correlation between Cu(II) sorption capacity and attachment efficiency in δ-MnO_2 system.

concentrations led to a corresponding decrease in the adsorption efficiency by shielding the surface charge, as shown in Fig. S1. The degree of Cu(II) uptake was lower in $CaCl_2$ than in NaCl, which could be explained by stronger competition between Ca^{2+} and Cu(II) for the surface adsorption sites of δ-MnO_2.[38] There was a notable decrease in the adsorption percentage when HA and $CaCl_2$ coexisted, but not in NaCl. This might be attributed to the enhanced aggregation of δ-MnO_2 in the presence of both HA and Ca^{2+} because the aggregation of nanoparticles would reduce the available surface area for the adsorption of metal ions.[13] Indeed, we found a good linear relationship of Cu(II) sorption efficiencies with an aggregation term, attachment efficiency (R^2 = 0.818) (Fig. 5). The observed negative correlation indicates that δ-MnO_2 aggregation leads to a decrease in Cu(II) uptake. Herein we successfully derived the relationship between sorption capacities and aggregation properties of δ-MnO_2, which may provide a basis for predicting the metal uptake under certain conditions. As a result, the surrounding water conditions that determine the process and state of nanoparticle aggregation strongly affect their ability to adsorb and sequester heavy metal ions.

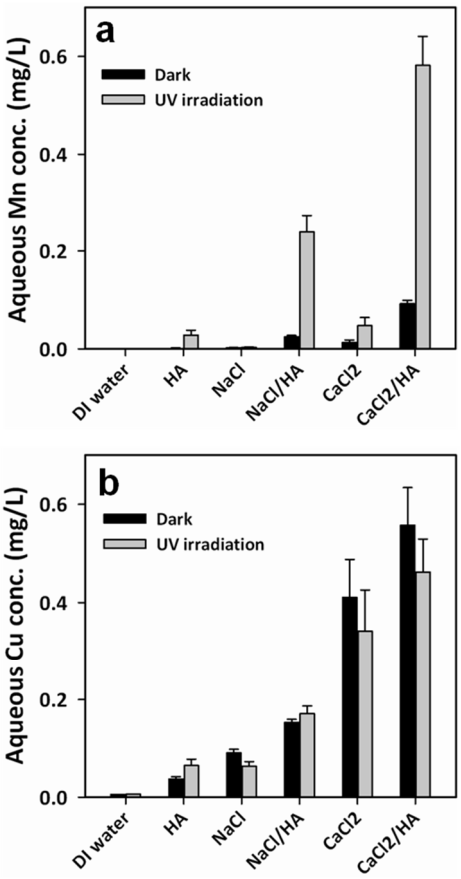

Fig. 6 Concentrations of dissolved (a) Mn and (b) Cu from Cu(II)-bearing δ-MnO_2 in the presence of various solutes under UV light irradiation for 10 h at pH 6.2 ± 0.2. Dissolution in the dark condition was compared. The concentrations of NaCl, $CaCl_2$, and HA were 100 mM, 10 mM, and 1 mg/L DOC, respectively.

Light-induced desorption of Cu(II) in synthetic water matrices

It has been reported that the dissolution of metal oxides occurs under both irradiation and dark conditions.[18,39-41] This phenomenon can affect the mobility and bioavailability of heavy metal ions trapped in metal oxides. Therefore, we studied the dissolution of δ-MnO_2 and concomitant desorption of Cu(II) under various water conditions in the absence and presence of UV light (Fig. 6).

As shown in Fig. 6a, the dissolution of δ-MnO_2 was negligible in DI water under both irradiated and dark conditions. However, the addition of HA caused the release of Mn from δ-MnO_2 in the light. This could be ascribed to the photoinduced ligand-to-metal charge transfer (LMCT, electron transfer from HA to Mn(IV)) or bandgap excitation (BE, electron transfer from valence bond to conduction band of MnO_2 and subsequently to Mn(IV)) with HA acting as a hole scavenger.[18,39] The photodissolution of δ-MnO_2 was synergistically enhanced in the presence of both electrolyte and HA. The adsorption of Na^+ or Ca^{2+} on the surface of δ-MnO_2 could reduce its negative surface charge, and thus enhance the adsorption of anionic HA. As a result, the release of Mn from δ-MnO_2 through LMCT and BE mechanisms, which essentially require the adsorption of HA, should be more favored in presence of electrolytes.

Light irradiation not only enhance the desorption of Cu(II) through the photoreductive dissolution of MnO_2 (reaction 1), but hinder it by making the surface charge of MnO_2 to more negative due to the accumulation of trapped conduction band electrons (reaction 2).[42]

$$\equiv Mn(IV) \xrightarrow{UV} Mn(II)_{aq} \quad (1)$$

$$\equiv Mn^{IV}\text{-}O]^{(4/3)-} \xrightarrow{UV} \equiv Mn^{III}\text{-}O]^{(7/3)-} \quad (2)$$

(The surface charge is determined by assuming that the surface Mn (with +4 formal charge) is located at the octahedral site surrounded by five lattice oxygen atoms and one surface group.)

To investigate the effect of light on the desorption of Cu(II), the results of Cu(II) release under dark and irradiated conditions were compared (Fig. 6b). In the absence of an electrolyte and HA, very little desorption of Cu(II) occurred in both conditions in accordance with the negligible dissolution of δ-MnO_2. However, the presence of HA appeared to slightly increase the Cu(II) desorption because HA competes with Cu(II) for the adsorption sites of δ-MnO_2. Particularly, the amount of desorbed Cu(II) in the light was higher than that in the dark, which could be attributed to the photoreductive dissolution of δ-MnO_2. On the contrary, the photoinduced desorption of Cu(II) was lower than in the dark in the presence of NaCl. Since the dissolution of δ-MnO_2 by light was negligible in NaCl, its effect on the desorption of Cu(II) can be ruled out. It appears that a more negatively charged δ-MnO_2 surface by reaction 2 pulls Cu(II) ions more strongly, and thus reduces the desorption of Cu(II). In addition, Mn(III) in the structure generated from reaction 2 might increase the

complexation affinity to Cu(II).[43] The presence of Ca^{2+} also reduced the desorption of Cu(II) like the case of Na^{+}.

When NaCl and HA are present together, the two irradiation effects (reactions 1 and 2) influence the desorption of Cu(II) in a complex manner resulting in the higher desorption of Cu(II). However, in $CaCl_2$, the effect of HA on the light-induced desorption of Cu(II) was not pronounced even though the dissolution of δ-MnO_2 with Ca^{2+} and HA was more significant than that with Na^{+} and HA. As exposed to light, HA can be degraded via LMCT and BE processes. A recent study also demonstrated that irradiation caused the destruction of electron donating moieties of HA.[44] When HA is adsorbed on the surface of MnO_2, the electrons in HA should be preferentially transferred to the conduction band or valence band holes of MnO_2, which initiates the degradation of HA. Then, the degraded HA can easily desorb from the surface of δ-MnO_2. The higher photoreductive dissolution of MnO_2 in the presence of both Ca^{2+} and HA implies that more HA molecules are degraded, and thus more adsorption sites on δ-MnO_2 are regenerated compared to the case of Na^{+} and HA. Under this condition, the re-sorption of desorbed Cu(II) should be more favored onto the regenerated adsorption sites, thereby reducing the effect of HA on Cu(II) desorption through the photoreductive dissolution of δ-MnO_2.

Conclusions

In natural environments, MnO_2 is expected to exhibit notably different aggregation behaviors corresponding to the local solution chemistry. The observations made in this study, which used synthetic water matrices with a wide range of ionic compositions and/or HA, proposed that the aggregation state alters the sorption ability of δ-MnO_2 toward Cu(II). δ-MnO_2 showed a reduced sorption capacity under favorable aggregation conditions, such as a high ionic strength and in particular those containing HA. However, the adsorbed Cu(II) could be released by the dissolution of δ-MnO_2 depending on the solution conditions and light irradiation even though the desorbed quantities were not significant. This work has broad environmental implications because heavy metal ions are mostly associated with various minerals in natural systems. Therefore, further dissolution studies with other types of minerals need to be addressed to better understand the long-term loading of heavy metals in the environment.

Acknowledgements

This work was supported by the National Research Foundation of Korea (NRF) grant funded by the Korea government (MEST) (No. 2011-0028723), and "The GAIA Project" by Korea Ministry of Environment.

Notes and references

[a] School of Environmental Science and Engineering, Pohang University of Science and Technology (POSTECH), Pohang, 790-784, Republic of Korea. E-mail: yschang@postech.ac.kr; Fax: +82-54-279-8299; Tel: +82-54-279-2281
[b] Department of Environmental Sciences and Biotechnology, Hallym University, Chuncheon, 200-702, Republic of Korea.

† Electronic Supplementary Information (ESI) available: Electrophorectic mobilities (EPMs) of δ-MnO_2 as a function of electrolyte concentrations in the absence and presence of HA; scheme of HA adsorption onto δ-MnO_2 and TiO_2; effect of pH on Cu(II) sorption percentage. See DOI: 10.1039/b000000x/

1 J. E. Post, *Proc. Natl. Acad. Sci. U. S. A.*, 1999, **96**, 3447−3454.
2 S. B. Kanungo, S. S. Tripathy and Rajeev, *J. Colloid Interface Sci.*, 2004, **269**, 1−10.
3 A. J. Frierdich and J. G. Catalano, *Geochim. Cosmochim. Acta*, 2012, **91**, 240−253.
4 E. J. Kim, C. S. Lee, Y. Y. Chang and Y. S. Chang, *ACS Appl. Mater. Interfaces*, 2013, **5**, 9628−9634.
5 O. Pourret and M. Davranche, *J. Colloid Interface Sci.*, 2013, **395**, 18−23.
6 B. J. Lafferty, M. Ginder-Vogel and D. L. Sparks, *Environ. Sci. Technol.*, 2010, **44**, 8460−8466.
7 S. J. Klaine, P. J. J. Alvarez, G. E. Batley, T. F. Fernandes, R. D. Handy, D. Y. Lyon, S. Mahendra, M. J. McLaughlin and J. R. Lead, *Environ. Toxicol. Chem.*, 2008, **27**, 1825−1851.
8 A. R. Petosa, D. P. Jaisi, I. R. Quevedo, M. Elimelech and N. Tufenkji, *Environ. Sci. Technol.*, 2010, **44**, 6532−6549.
9 N. Saleh, H. J. Kim, T. Phenrat, K. Matyjaszewski, R. D. Tilton and G. V. Lowry, *Environ. Sci. Technol.*, 2008, **42**, 3349−3355.
10 R. F. Domingos, N. Tufenkji and K. J. Wilkinson, *Environ. Sci. Technol.*, 2009, **43**, 1282−1286.
11 R. A. French, A. R. Jacobson, B. Kim, S. L. Isley, R. L. Penn and P. C. Baveye, *Environ. Sci. Technol.*, 2009, **43**, 1354−1359.
12 P. J. Vikesland, A. M. Heathcock, R. L. Rebodos and K. E. Makus, *Environ. Sci. Technol.*, 2007, **41**, 5277−5283.
13 B. Gilbert, R. K. Ono, K. A. Ching and C. S. Kim, *J. Colloid Interface Sci.*, 2009, **339**, 285−295.
14 K. D. Kwon, K. Refson and G. Sposito, *Geochim. Cosmochim. Acta*, 2009, **73**, 4142−4150.
15 Q. Li, B. Xie, Y. S. Hwang and Y. Xu, *Environ. Sci. Technol.*, 2009, **43**, 3574−3579.
16 S. W. Bennett, D. Zhou, R. Mielke and A. A. Keller, *PLoS ONE*, 2012, **7**, e48719.
17 X. Li and J. J. Lenhart, *Environ. Sci. Technol.*, 2012, **46**, 5378−5386.
18 K. Kim, H. -I. Yoon and W. Choi, *Environ. Sci. Technol.*, 2012, **46**, 13160−13166.
19 G. Landrot, M. Ginder-Vogel, K. Livi, J. P. Fitts and D. L. Sparks, *Environ. Sci. Technol.*, 2012, **46**, 11601−11609.
20 K. L. Chen and M. Elimelech, *Langmuir*, 2006, **22**, 10994−11001.
21 L. H. Slooff, S. C. Veenstra, J. M. Kroon, W. Verhees and L. J. A. Koster, *Phys. Chem. Chem. Phys.,* 2014, **16**, 5732−5738.
22 M. Villalobos, B. Lanson, A. Manceau, B. Toner and G. Sposito, *Am. Mineral.*, 2006, **91**, 489−502.
23 T. Gao, M. Glerup, F. Krumeich, R. Nesper, H. Fjellvåq and P. Norby, *J. Phys. Chem. C*, 2008, **112**, 13134−13140.
24 S. E. Fendorf and R. J. Zasoski, *Environ. Sci. Technol.*, 1992, **26**, 79−85.
25 C. L. Peacock and D. M. Sherman, *Chem. Geol.*, 2007, **238**, 94−106.
26 M. Villalobos, B. Lanson, A. Manceau, B. Toner and G. Sposito, *Am. Mineral.*, 2006, **91**, 489−502.
27 M. Zhu, C. L. Farrow, J. E. Post, K. J. T. Livi, S. J. L. Billinge, M. Ginder-Vogel and D. L. Sparks, *Geochim. Cosmochim. Acta*, 2012, **81**, 39−55.
28 S. E. Mylon, K. L. Chen and M. Elimelech, *Langmuir*, 2004, **20**, 9000−9006.
29 K. L. Chen, S. E. Mylon and M. Elimelech, *Environ. Sci. Technol.*, 2006, **40**, 1516−1523.
30 A. A. Keller, H. Wang, D. Zhou, H. S. Lenihan, G. Cherr, B. J. Cardinale, R. Miller and Z. Ji, *Environ. Sci. Technol.*, 2010, **44**, 1962−1967.
31 J. W. Murray, *Geochim. Cosmochim. Acta*, 1975, **39**, 505−519.
32 B. J. R. Thio, D. Zhou and A. A. Keller, *J. Hazard. Mater.*, 2011, **189**, 556−563.
33 S. Ghosh, H. Mashayekhi, B. Pan, P. Bhowmik and B. Xing, *Langmuir,* 2008, **24**, 12385−12391.
34 J. Chorover and M. K. Amistadi, *Geochim. Cosmochim. Acta*, 2001, **65**, 95−109.
35 T. Martinez, C. Romero and J. M. Gavilán, *Fuel*, 1983, **62**, 869−870.

36 E. Tipping and M. Ohnstad, *Nature*, 1984, **308**, 266−268.
37 K. L. Chen and M. Elimelech, *J. Colloid Interface Sci.*, 2007, **309**, 126−134.
38 M. Zhu, M. Ginder-Vogel, S. J. Parikh, X. -H. Feng and D. L. Sparks, *Environ. Sci. Technol.*, 2010, **44**, 4465−4471.
39 K. Kim, W. Choi, M. R. Hoffmann, H. -I. Yoon and B. -K. Park, *Environ. Sci. Technol.*, 2010, **44**, 4142−4148.
40 J. F. Perez-Benito and C. Arias, *J. Colloid Interface Sci.*, 1992, **149**, 92−97.
41 D. Jeong, K. Kim and W. Choi, *Atmos. Chem. Phys.*, 2012, **12**, 11125−11133.
42 W. W. Dunn, Y. Aikawa and A. J. Bard, *J. Am. Chem. Soc.*, 1981, **103**, 3456−3459.
43 M. Zhu, M. Ginder-Vogel and D. L. Sparks, *Environ. Sci. Technol.*, 2010, **44**, 4472−4478.
44 C. M. Sharpless, M. Aeschbacher, S. E. Page, J. Wenk, M. Sander and K. Mcneill, *Environ. Sci. Technol.*, 2014, **48**, 2688−2696.